The effect of systemic lipopolysaccharides on the cardiovascular system in Sprague-Dawley rats using Manuka honey as a treatment

Glory Isabella Tambwe[1], Sajee Alummoottil[1], * Chantelle Venter[2], Janette Bester[1]

[1]Department of Physiology, University of Pretoria, Pretoria 0007, South Africa

[2]Department of Physiological Sciences, Faculty of Science, Stellenbosch University, Stellenbosch, Private Bag X1 Matieland, 7602, South Africa.

***Corresponding authors:**

Dr Janette Bester:

Physical address: Department of Physiology Faculty of Health Sciences, University of Pretoria, Private Bag X20, South Africa

Email address: Janette.bester@up.ac.za

Tel: (+27) 319 2679

Abstract

Background: It has been said that there is a probable “head-to-heart” link in resulting in the development of Alzheimer’s disease (AD). This is because cardiovascular (CV) and neurodegenerative diseases such as AD share many risk factors. Researchers have theorised that a significant contributor to the neurological and CV complications in AD may be due to exposure to the lipopolysaccharide (LPS) endotoxin that results in a low-grade systemic inflammatory immune response. Systemic inflammation impacts both the CV and neurological systems in harmful ways. The elderly is more vulnerable to exposure since they are increasingly likely to suffer from tooth loss or gastrointestinal tract impairments resulting in LPS introduction into the CV system.

Aim: The aim of the study was to investigate the effect of low physiological levels of systemic LPS exposure on the CV system, of male Sprague-Dawley rats over a ten-day period. Manuka honey was introduced as a possible mopping agent for the effects of LPS on the CV system.

Study design: Twenty-four 10-week-old male Sprague-Dawley rats (average weight: 250-300 g) were randomly divided into four groups. The groups included rats exposed to Phosphate buffer-saline, phosphate buffered-saline and Manuka honey, LPS only as well as LPS and Manuka honey. The animals were housed for 19 days, in which the animals were given daily subcutaneous injections. The Manuka honey administered to the control and experimental groups received the Manuka honey solution through oral gavage starting on the 11th day for a seven-day period.

Methods: In this study we examined the CV tissue of the animals through light microscopy and transmission electron microscopy. The total cholesterol levels were also measured by using the QuickDetect^{TM} total cholesterol (Rat) ELISA assay.

Results: Myocardial LPS exposure resulted in cardiac myofibril damage and mitochondrial cristae destruction. The results indicated that Manuka honey may have alleviated some of this damage. However, the treatment failed to prevent mitochondrial cristae destruction. Lipopolysaccharide exposure to aortic tissue resulted in cellular abnormalities, elastic fragmentation and collagen deposition. Manuka honey administration resulted in the reduction of cellular abnormalities and elastin fragmentation in the aorta however, the treatment induced collagen depletion.

Conclusion: The aorta and cardiac muscle are vulnerable to the effects of low levels of systemic LPS exposure. Exposure resulted in elevation in cardiac and aortic cellular and elastin destruction that may possibly conclude in CV disease long term. In addition, Manuka

honey serves as an insufficient remedy to counteract the harmful effects of LPS on the CV system.

Keywords: Aorta, cardiovascular disease, lipopolysaccharide, Manuka honey, neurodegeneration.

Introduction

Alzheimer's disease is categorised as a neurological disease that effects middle and old aged individuals. There is accumulating evidence suggesting that the pathogenesis is not confined to a neurological cause (1). Neurological and cardiovascular (CV) diseases share risk factors such as blood pressure, cholesterol, obesity, glucose control, and chronic inflammation (2, 3). These CV risk factors are also associated with an elevation of cognitive impairment and dementia. Although the underlying explanation of this association is unclear, inflammation plays a central role in CV and neurodegenerative disease aetiology (4, 5). Nevertheless, studies have found that there is a link between cognitive impairment and heart failure through angiopathy, inflammation and perfusion defects, regardless of if a patient presents with AD (6). Lipopolysaccharide (LPS) exposure results an inflammatory response that plays a crucial role in neuropsychiatric dysfunction in rodents (7). This study proposes Manuka honey as a possible treatment for the systemic inflammatory effects of LPS because of its anti-inflammatory, anti-oxidant and wound healing properties (8). In addition, Manuka honey results in hydrogen peroxide release that is antibacterial, and its unique advantageous antibacterial manuka factor (methylglyoxal) that aids in heal wounds (8). This study investigates if the manuka factor reduces systemic inflammation in the test subjects.

Previous studies have suggested that infectious agents may be responsible for the development of AD, as emerging evidence has shown that the gastrointestinal microbiome affects neurodegenerative disease development and progression. Lipopolysaccharides form the majority of the outer membrane's outer leaflet in gram-negative bacteria (i.e., *E. coli*), and fulfil two functions. Firstly, it protects the bacteria from harsh environments (9, 10).This occurs in the following manner: the toxin acts as a barrier against stress factors which makes LPS indispensable for bacterial variability in stressful environments (11). Uncontrolled bacterial growth within human bodies (GIT with leaky guts or tooth loss resulting in entry or within the CV as seen in sepsis) leads to large LPS quantities which can result in an overstressed systemic host immune response (10). Lipopolysaccharides release many pro-inflammatory cytokines such as interleukin-1β (IL-1β) and tumour necrosis factor alpha (TNFα) (12, 13). Interleukin-1β is vital to the oxidative and neuroinflammatory responses bought about by LPS and has been identified as a key mediator in behavioural dysfunction found in rodents (7, 12). This may be attributed to LPS secretions from dormant gram-negative bacteria such as *E. coli* as that reside in the systemic circulation (14). Systemic inflammation found in dementia patients (more specifically AD patients) may affect the entire body and stem from mild exposure to a bacterial toxin (14).

In addition, the endotoxin has been shown to have CV effects such as inducing atherosclerosis and cardiomyocyte autophagy (15, 16). Recent studies have found that LPS exposure induces myocardial inflammation leading to cardiotoxicity due to acute inflammation as seen in figure 1 systemic inflammation results in cardiotoxicity as disrupts multiple organs (20). This study forms part of a larger study that investigates the effects of the systemic inflammatory effects of LPS on the heart, liver and brain.

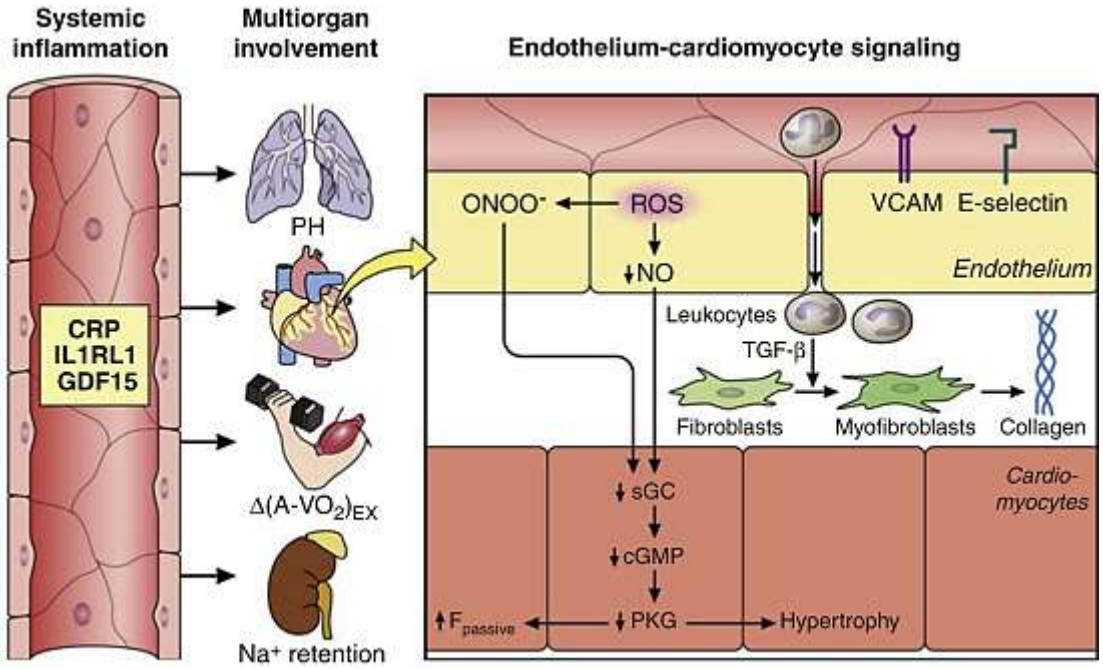

Figure 1: The effect of systemic inflammation on the heart and other organs- Systemic inflammation results in multiple organ dysfunction such as the kidney, heart etc. In addition, chronic systemic inflammation results in hypertrophy of the cardiomyocytes which may result in cardiac dysfunction.

In addition, systemic inflammation disrupts erythrocyte, platelet and fibrin network structure (21). This instance may result in hypoperfusion (16). A study conducted by Roher et al. (2012) observed that AD patients experienced 20% lower cerebral blood flow than a control group, suggesting a connection between AD dementia and brain hypoperfusion (17). Furthermore, hypercholesteremia is associated with an elevated CV dysfunction and AD risk (18). Hypercholesteremia is also associated with atherosclerosis since the condition is induced by an inflammatory process that is characterised by oxidised low-density lipoprotein (LDL) deposition, endothelial cell injury and vascular wall plaque accretion (19). Alzheimer's disease and atherosclerosis are significantly related to one another. Experimental studies have also shown that gut-derived LPS are proatherogenic and may therefore further enhance the negative effects of elevated LDL cholesterol levels (20).

There are very few studies that have studied the relationship between AD and CV disease therefore there is a need to better understand the nature of disease interactions and to identify preventive measures for reducing CV risk in this specific population (21). The Manuka factor has successfully treated Escherichia coli (*E. coli*) derived LPS, which induces systemic inflammation, and that was the rationale in using it as a treatment in this study(8, 22, 23). The aim of the study was the following to investigate the *in vivo* effect that systemically induced LPS has on the well-being, behaviour, memory and the CV system, of ten-week-old male Sprague-Dawley rats and the effect of Manuka honey as a treatment. This study investigated the effect of low physiological levels of LPS on the CV system that is similar to what is expected in an AD population. The study also investigated Manuka honey as a possible mopping agent for the effects of LPS on the CV system.

Methods

Ethical statement

This study received ethical approval from the University of Pretoria Animal Ethics (protocol number: 171-2020) and the University of the Witwatersrand's Animal ethics committee (protocol number: 2019/07/44C).

Study design

Twenty-four 10-week-old male Sprague-Dawley rats (average weight: 250-300 g) were used in this study. The animals were housed at the University of the Witwatersrand Central Animal Service (CAS) unit where they were randomly divided into two control and two experimental groups. Each group contained six rats. Table 1 represents the animal groups and the doses administered.

Table 1: Animal groups and treatment administration

Animal study	
Vehicle control	Formulation: 0.1M at volume of 0.1mg/ml
PBS + Honey (H)	PBS Formulation: 0.1M at volume of 0.1mg/ml Manuka honey dilution: 50:50 honey and distilled water
LPS (Sigma-Aldrich)	Dose: SC LPS *E. coli* (at 0.1.mg/ml at a volume of 0.5mg/kg of the rat)
LPS + Honey (H)	LPS Dose: SC LPS *E. coli* 055: B5 (at 0.1.mg/ml at a volume of 0.05mg/kg of the rat) Manuka honey dilution: 50:50 honey and distilled water

The test subjects were housed in cages with sizes laid down per the SANS 10386:2008 recommendations in the following conditions: room temperature 25-27 ˚C (±2 ˚C), relative 50% (± 20%) humidity and a 12-hour night/dark cycle. The test subjects were acclimatised for seven days prior to dosage administration. Following that, the ten-day experimental period occurred. The rats were weighed daily and the weight of the rat determined the dose the test subject received. Honey was administered to the treated control and experimental group through oral gavage on the 11th day for a seven-day period. There were no significant weight changes during the course of the study. Termination took place on day 19 through cardiac puncture followed by saline perfusion. During termination the cardiac tissue samples were harvested. All the tissue was stored at room temperature in 4% formaldehyde for 24 hours. After sample preparation, the organs were studied using Light microscopy (LM) and Transmission electron microscopy (TEM) as well as determination of the total cholesterol through a QuickDetect^{TM} total cholesterol (Rat) ELISA kit. All the sample preparations and analyses took place at the University of Pretoria Physiological laboratory and the Laboratory for Microscopy and Microanalysis.

Light microscopy

Preparation

The hearts and aorta were longitudinally and transversely sectioned and fixed in the 4% formaldehyde. The samples were fixed for 24 hours at room temperature before the tissue

samples were rinsed with 0.1 M PBS three times for 30 minutes. Following the rinsing, the samples were dehydrated with 50% ethanol for 30 minutes, 70% ethanol for an hour, 90% ethanol for an hour and lastly the samples were dehydrated twice in 100% ethanol for an hour. The samples were then placed in 100% ethanol overnight. The following day, the samples were treated with 50% xylene in ethanol for 30 minutes. Following that the samples were placed in xylene for two hours. The samples were also placed in 30% parafilm wax and 70% xylene mixture for an hour at a temperature of 60˚C then in a 70% wax and 30% xylene mixture for an hour at a temperature of 60˚C and lastly in 100% wax for two hours at a temperature of 60˚C. Finally, the tissue was sectioned using the Leica RM 2255 microtome then placed on warm water at 45 ˚C in the Thermo scientific section flotation bath, then mounted on glass slides before being placed on the Raymond A lamb slide warmer to dry at 45˚C.

Haemoxylin and Eosin

The stain was used to compare the cardiomyocyte and aortic cell morphology through the comparison of nuclei, cytoplasm and connective tissue fibres of the experimental, treated experimental, control and treated control group.

The process was the following, the wax slides were emersed in xylene for ten minutes. Following that, the slides were placed in xylene for five minutes. If the slides still contained wax, the slides remained in the xylene for an additional five minutes. The samples were then placed in series of ethanol concentrations: 100% ethanol for four minutes, following that, 90% ethanol for one minute, and lastly in 70% ethanol for one minute. Following that, the slides were placed distilled water for one minute.

The sections were then placed in Haematoxylin (Sigma-Aldrich) for 15 minutes. The glass slides were then placed in Scott's buffer for eight minutes. Following that, the samples were repeatedly submerged in distilled water for ten seconds then dipped in 1% eosin. The glass slides were again rinsed in distilled water for one minute. The slides were briefly submerged in 70%, 90%, 100% ethanol, and then xylene. Following that, the samples were allowed to air dry and then mounted with Entellan® mounting media (Merck) and a coverslip was placed over the samples. Micrographs were captured using the Zeiss AXIO Imager.M2 light microscope (Carl Zeiss Microscopy, Munich, Germany).

Periodic acid-Schiff

The Periodic acid-Schiff (PAS) staining method identifies carbohydrates or glycoconjugates, table 2 lists PAS reactive tissue and cell components.

Table 2: Periodic Acid-Schiff reactive tissue and cell components

Markers identified
Glycogen (specific to cardiomyocytes)
Starch
Mucin (sialomucin, neutral mucin)
Basement membranes
α-antitrypsin
Reticulin
Fungi (capsules)
Pancreatic zymogen granules
Thyroid colloid
Corpora amylacea
Russel bodies

The stain reacts to the free aldehyde groups within the carbohydrates and the Schiff reagent reacts with the free carbohydrate aldehyde groups that result in a bright red or magenta end product concluding in polysaccharide identification (24). Glycogen cardiomyocyte presentation is of primary interest in this study (24). The Schiff reagent's glycoprotein reactivity within the basal lamina results in the PAS technique which is extremely valuable in basement membrane width assessment (25). Increased basement membrane thickness occurs in a number of pathological conditions (24). More specifically, the technique will identify cardiomyocyte hypoxia or normoxia depending on the colour displayed. During cardiomyocyte normoxia, a low glycogen accumulation rate is maintained and the cells are stained purple. During hypoxia, an elevated glycogen content would present in the cardiomyocytes thus the cells would stain bright or magenta while employing the PAS staining method (26). The technique investigated if LPS induces cardiomyocyte hypoxia and if Manuka honey is an effective treatment.

The staining process was conducted in the following was: the PAS kit has working chemical reagents that were pre-concocted for use. The cardiac muscle sections were deparaffinised as previously described and hydrated in distilled water. The slides were immersed in Periodic Acid Solution for five minutes at room temperature and then rinsed in distilled water then immersed Schiff's reagent for 15 minutes at room temperature. The slides were rinsed with running tap water for five minutes then counterstained in Haematoxylin Solution (Gill no 3) for

90 seconds. After this the slides were rinsed with running tap water. Then dehydrated with 70%, 90%, and 100% ethanol then xylene. The slides were cleared and mounted with Entellan® mounting media. The samples were viewed using the Zeiss AXIO Imager.M2 light microscope (Carl Zeiss Microscopy, Munich, Germany).

Verhoeff-Van Gieson

Verhoeff-Van Gieson (VVG) is a histochemical stain which enables the visualisation of elastic fibres, identification of normal and abnormal (pathological) aortic elastic fibres differentiation (27). Elastic fibres are one of the connective tissue types and their main function is to provide elasticity and flexibility. As a result any abnormalities in blood vessel wall elasticity concludes in pathology (28). Abnormal elastic fibre pattern detection aids in pathological condition diagnose (28).

The staining process was conducted in the following way: The aorta wax sections were deparaffinized (as previously described) and hydrated in distilled water. The slides were placed in a working elastic stain solution for five minutes then rinsed in running tap water. Following that, the slides were dipped in differentiating Ferric Chloride solution for 30 seconds and then rinsed in tap water. The slides were checked microscopically to determine correct colour appearance and if the targeted structures could be correctly identified. If the samples were over differentiated (Ferric Chloride produced an overpowering colour) the samples were returned to the working elastic stain solution. The slides were rinsed in 95% ethanol to remove the iodine(29). Following that, the slides were rinsed with running tap water and then stained with in Van Gieson Solution for one minute. The slides were then rinsed in 95% ethanol and dehydrated with xylene. The slides were cleated and mounted in Entellan® mounting media (Merck 12 Gaa) and viewed using Zeiss AXIO ImagerM2 light microscope (Carl Zeiss Microscopy, Munich, Germany).

Transmission electron microscopy

The heart and aortic tissues were cut into $5mm^3$ blocks then fixed in 4% formaldehyde solution for 24 hours. The fixative solution was removed and the samples underwent three, 15-minute, 0.1 M PBS buffer washes. After the third buffer wash a 1% osmium tetroxide solution was added to complete the fixation step. The sample remained in the osmium tetroxide for an hour. Following that, the sample was washed again three times with PBS, for 15 minutes each. The samples were dehydrated in a series of 30%, 50%, 70%, 90% ethanol then three times in 100% ethanol. Each dehydration step had a 15-minute duration.

The infiltration process had two steps: a two to one Ethanol: Agar 100 resin mixture (add manufacturer info) was added to the samples for an hour followed by a one to two Ethanol: Agar 100 resin mixture for two to four hours. The ethanol resin solution was removed. One

hundred percent Agar 100 resin was added to the samples for 4 hours before it was embedded into rubber moulds. The embedded samples were placed in an oven for 36 hours at 60˚C for polymerization. Following the 36-hour period, the samples were removed from the oven and cut into semi-thin sections (0,35 µm) with the ultramicrotome That was placed on glass slides and stained with Toluidine blue then samples were cut into ultra-thin (80-100 nm) sections and placed onto copper grids, stained with uranyl acetate and lead citrate for contrast. The stained samples were viewed using a JEOL JEM 2100F TEM (JEOL Ltd., Tokyo, Japan).

Statistical analysis: Total cholesterol ELISA

The total cholesterol test was utilised because the total cholesterol concentration in the CV system gives an indication of a cholesterol homeostasis disruption. Such a disruption indicates the effect of LPS on cholesterol regulation as well as the ability of Manuka honey to treat the disruption.

The test proceeded as follows: The QuickDetect™ total cholesterol (Rat) ELISA (Biovision kit: K4436-100) was used: The reagents, samples, and standards solutions were prepared according to manufactures instructions which were as follows: 40 µl of sample dilution buffer and 10 µl were added into the wells (the dilution factor of five). Seven samples from each group were used and later compared, the samples were tested twice. One well remained empty as a blank control. Following that, the blood serum samples were loaded onto the bottom without touching the well walls and the wells were gently shaken on a plate shaker. The samples were sealed and incubated for 30 minutes at 37 ˚C. After the incubation the seal were removed and the samples were aspirated and refilled with the wash solution. The washing procedure was repeated five times. Fifty microlitres of Horseradish Peroxidase (HRP)-Conjugate reagent was added to each well, except the blank control well and incubated for 30 minutes at 37 ˚C. Following that, the samples were aspirated and refilled with wash solution. The washing procedure was repeated five times. Following that, 50 µl of Chromogen Solution A and 50 µl Chromogen Solution B were added to each well. The samples were then mixed by gently shaking the well and incubated in the dark at 37 ˚C for fifteen minutes. Fifty microlitres of stop solution was added to each well to terminate the reaction. The colour in the well changed from blue to yellow. The absorbance readings were processed using Gen 5™ plate reader software, fifteen minutes after adding stop solution. The OD value for the blank control well was set as zero.

Results

Light Microscopy

Cardiac Muscle

The aortic and cardiac tissue histology and ultrastructure were documented and compared using light microscopy and TEM, respectively. Haematoxylin and Eosin allowed for the identification and documentation of normal or pathological cardiomyocyte and aortic cell morphology. An overview of the cardiac myofibril of the control and experimental groups are shown in figure 2. The myofibrils displayed by the control and treated control groups (as seen in figure 2 A and B) displayed a normal organised myofibril arrangement at low magnification. High myofibril magnification of the control and treated control group displayed oval centralised nuclei that contained blood vessels and capillaries. The experimental and treated experimental group displayed oval nuclei. In addition, the experimental group as seen in figure 2 C displayed myofibril damage and erythrocyte extravasation. The treated experimental group (figure 2 D) showed myofibril damage.

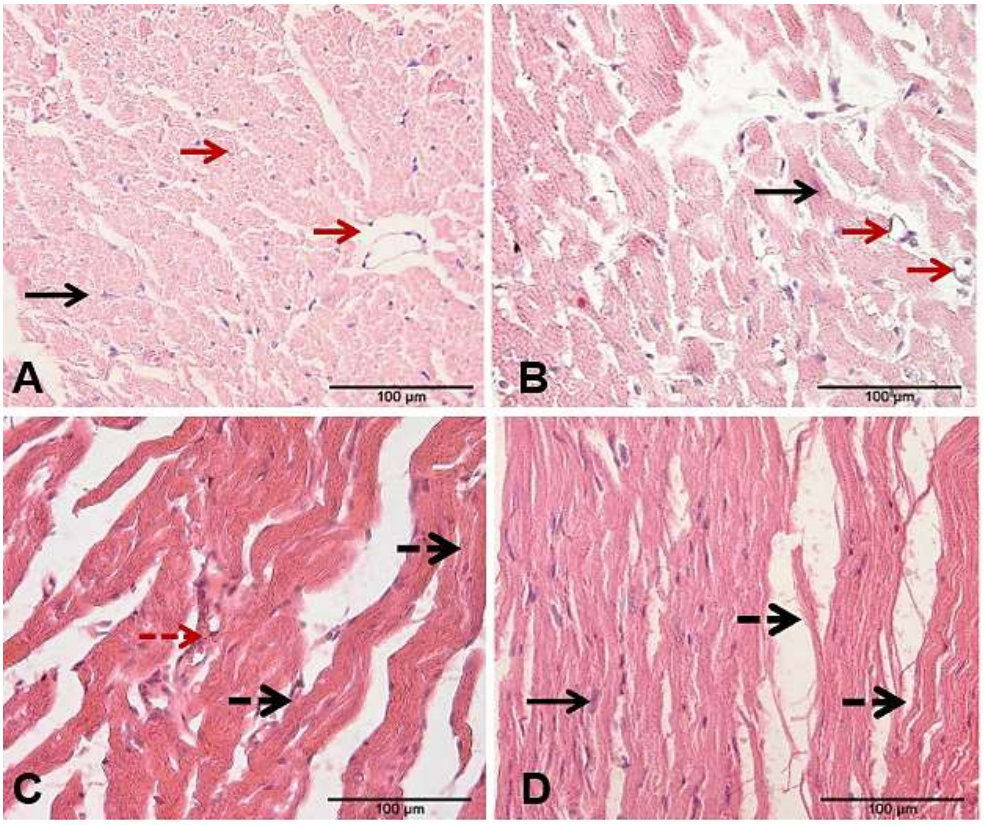

Figure 2: Haematoxylin and Eosin cardiac muscle section- Figure A (control), Figure B (treated control), Figure C (experimental), Figure D (treated experimental). The images display a detailed image of the common condition of the cardiovascular tissue found in each group. Black arrow: Oval and centrally located nuclei, Black dashed arrow: Myofibril damage. Red arrow: Blood vessel and capillaries. Red dashed arrow: Erythrocyte extravasation (Scale bar: 100µm).

The PAS technique provides a visual representation of the glycogen content in the tissues. The following images are of the control and experimental cardiac tissue specimens. A low glycogen concentration is expressed as a light purple colour. All of the control and experimental specimens as shown in figure 3 displayed normal glycogen content.

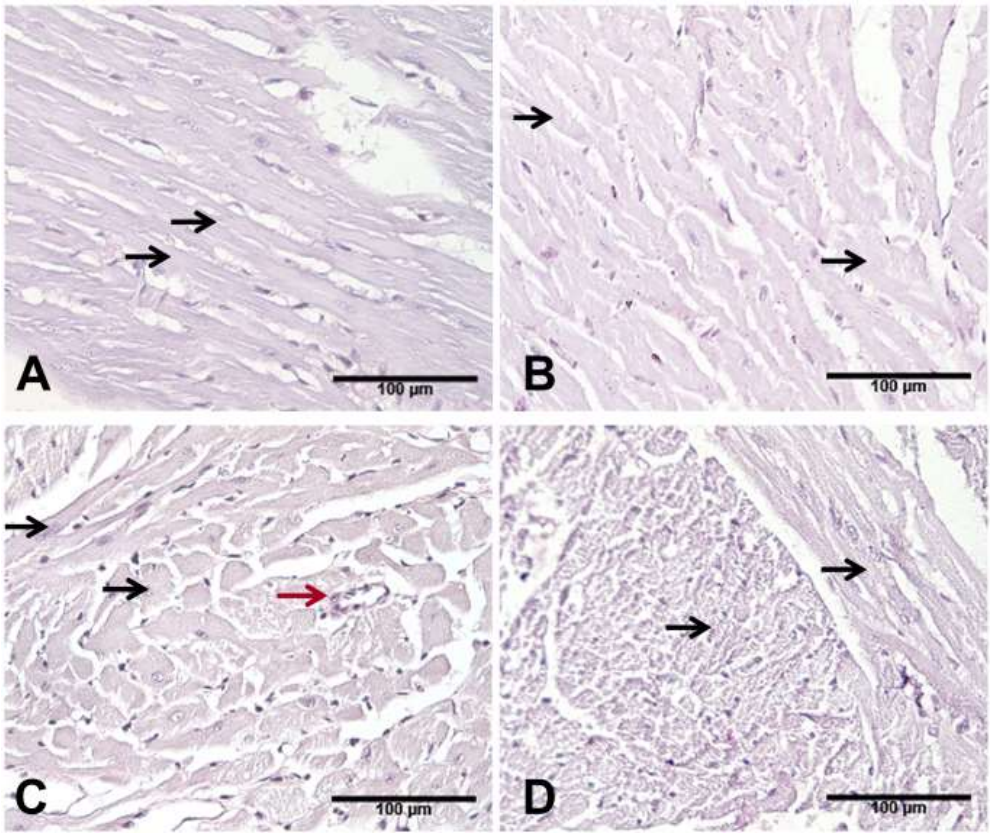

Figure 3: Periodic Acid-Schiff cardiac muscle section- Figure A (control), Figure B (control treated), Figure C (experimental), Figure D (experimental treated). Low glycogen content expresses itself as a light purple while a high glycogen content is seen as dark purple. Key: Black arrow: Low glycogen content. Red arrow: High glycogen content (Scale bar: 100µm)

Aorta

The control and experimental group aortic tissue specimens were stained with the H and E (figure 4 A-D) and VVG (figure 6). Figure 4 and figure 5 provide an overview on the structural condition of the aortas found in each group. Upon tissue inspection on low magnification of the aortic tissue of the control and treated control groups, the aorta of the control group displayed normal morphology (Fig. 4A). When viewing the tissue on a higher magnification, the aorta of the control and treated control group displayed normal morphology which can be described as even aortic wall thickness with oval nuclei with a minute amount of perinuclear space. The experimental group showed both normal aortic morphologies however large degrees of tissue destruction in some areas, the destruction can be seen on a lower

magnification (Fig. 4C). When viewing the tissue on a higher magnification as seen in figure 5 C and D, both the experimental and treated experimental group displayed widely spread perinuclei while in other areas the nuclei were flattened and clustered together. Meanwhile, the treated experimental group displayed largely intact aortic tissue however upon closer examination cellular tissue destruction in what appears to be perforations that occurred (figure 4 D).

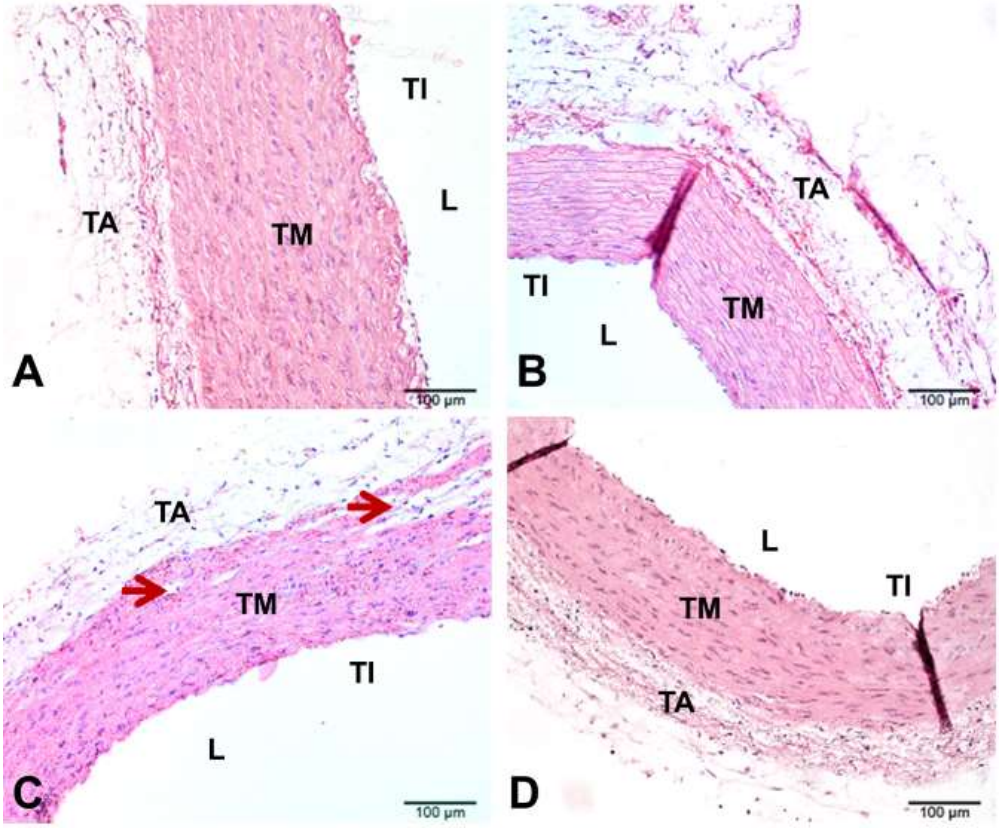

Figure 4: Haematoxylin and Eosin aorta sections- Figure A (control), Figure B (control treated), Figure C (experimental), Figure D (experimental treated). **Key:** L: Lumen. TA: Tunica Adventitia. TI: Tunica Intima. TM: Tunica Media Red arrow: Changes in tissue structure. (Scale bar: 100 µm)

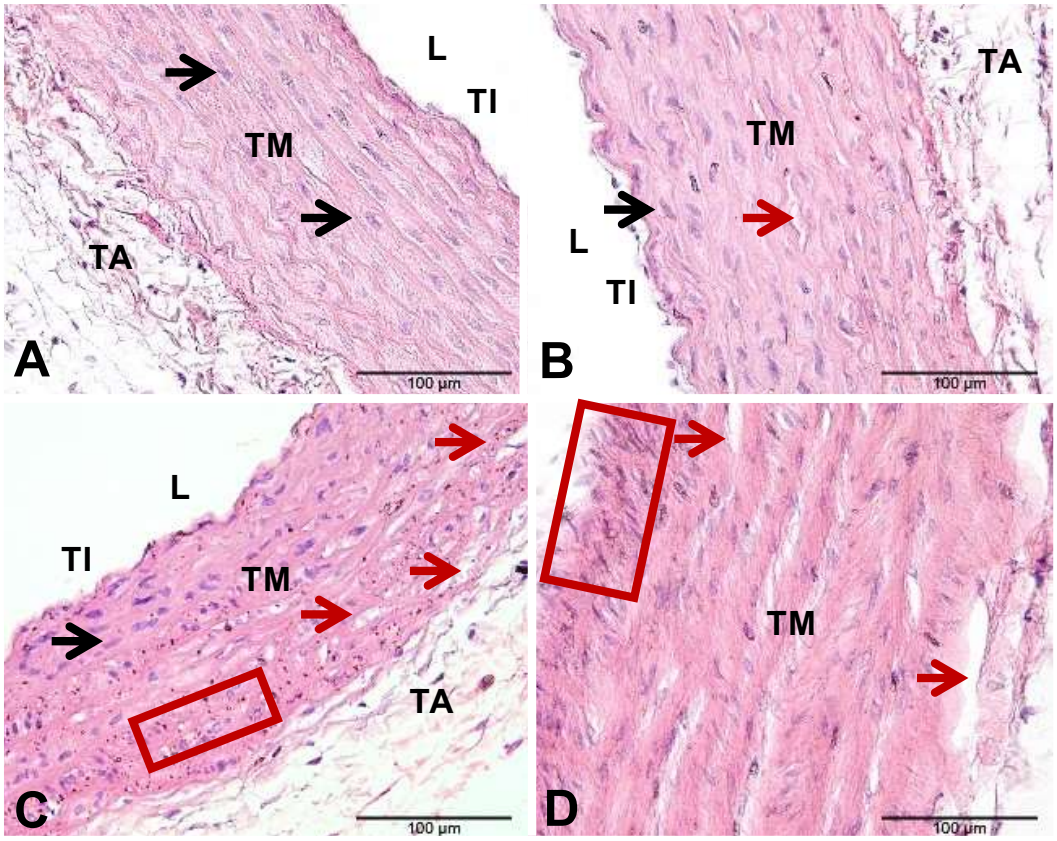

Figure 5: Haematoxylin and Eosin aorta sections- Figure A (control), Figure B (control treated), Figure C (experimental), Figure D (experimental treated). **Key:** L: Lumen. TA: Tunica Adventitia. TI: Tunica Intima. TM: Tunica Media. Red arrow: Changes in tissue structure. Red box: Noticeably clustered nuclei (Scale bar: 100 µm)

Figure 6 displays the aortic tissue of the control, control treated, experimental and treated experimental groups that were stained using the VVG technique. The control and treated control group showed evenly thick, regular arranged purple/black elastin brands strands that contained interlinkages between the elastic laminae as seen in figures 6 A and B. The experimental group displayed elastic bands that were unevenly thick and contained many interlinkages between the elastic laminae, displaying disordered elastic fibre arrangements as seen in figure 6 C. The treated experimental group displayed minor to moderate changes in elastic fibre arrangements and displayed interlinkages between the elastic laminae as seen in figure 6 D.

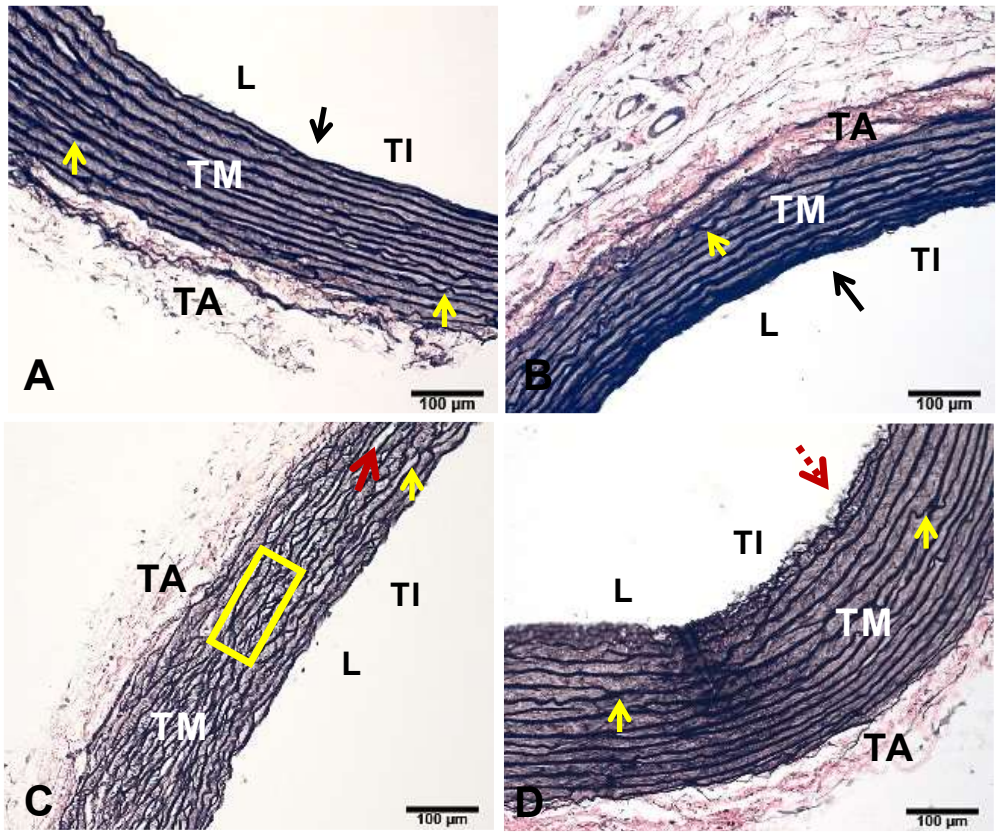

Figure 6: Verhoeff-Van Gieson aorta section- Figure A (control), Figure B (control treated), Figure C (experimental), Figure D (experimental treated). **Key:** L: Lumen. TA: Tunica Adventitia. TI: Tunica Intima. TM: Tunica Media. Black arrow: Tunica Intima changes. Yellow arrow: Crosslinks between elastic laminae. Yellow box: Major cell layer disruptions in the form of cross links. (Scale bar: 100µm)

Transmission electron microscopy

The ultrastructural morphology of the cardiac muscle mitochondria and myofibrils and the aorta collagen and elastin fibres of the control and experimental groups were studied using TEM.

Cardiac muscle

Longitudinal cardiac muscle sections allowed for cardiac myofibril ultrastructure observations and comparisons between the control, treated control, experimental and treated experimental groups as seen in figure 7 (A-D). Normal ultrastructure with well organised parallel mitochondrial and cardiac fibrils and clear Z lines (white arrows) was exhibited in the control and treated control groups (figure 7 A and B). While the experimental groups displayed minor damage and an elevated mitochondrial presence. Both the experimental groups displayed clear Z lines. However, the thinned cardiac myofibrils showed minor damage through Z line interruptions in the presence of enlarged mitochondria between cardiac muscle in both the experimental and treated experimental groups (figures 7 C and D). Minor mitochondrial destruction was illustrated by the red arrows. None of the groups had a presence of autophagic

vacuoles. The experimental group displayed myofibrils that showed moderate damage while the treated experimental group displayed minor cardiac myofibril damage.

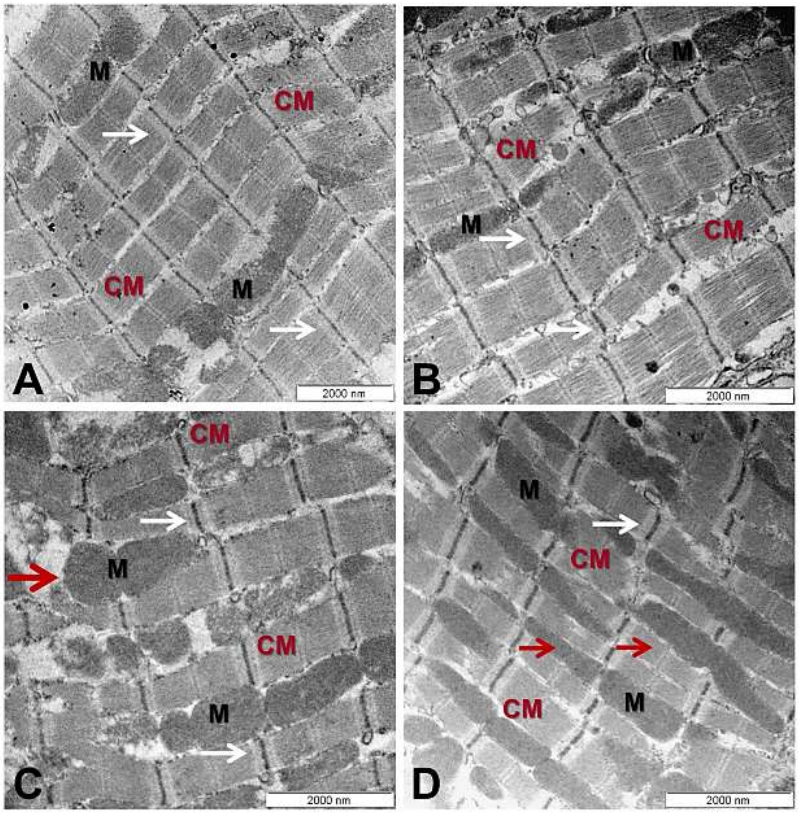

Figure 7: Representative micrographs of the ultrastructure of cardiomyocyte longitudinal sections- Figure A (control), Figure B (control treated), Figure C (experimental), and Figure D (experimental treated). CM: Cardiac myofibrils. M: Mitochondria. White arrow: normal Z-lines. Red arrow: Myofibril thinning and destruction (Scale bars: 2000nm)

The changes in mitochondrial shape are displayed in figure 8 (A-D) where the ultrastructure of control and experimental mitochondrial are displayed. The control groups displayed normal and healthy mitochondrial crista that were neatly and densely packed (figure 8 A and B), axial tubules are visible as the empty spaces in the tissues. Variations to standard cristae morphology to occur in the control groups but were rarities. While the experimental group presented less densely packed and neatly organised mitochondria signifying early mitochondrial damage in figures 8 C and D. The groups illustrated a variety of mitochondrial morphologies such as normal to minor damage as seen in figures 8 C and D.

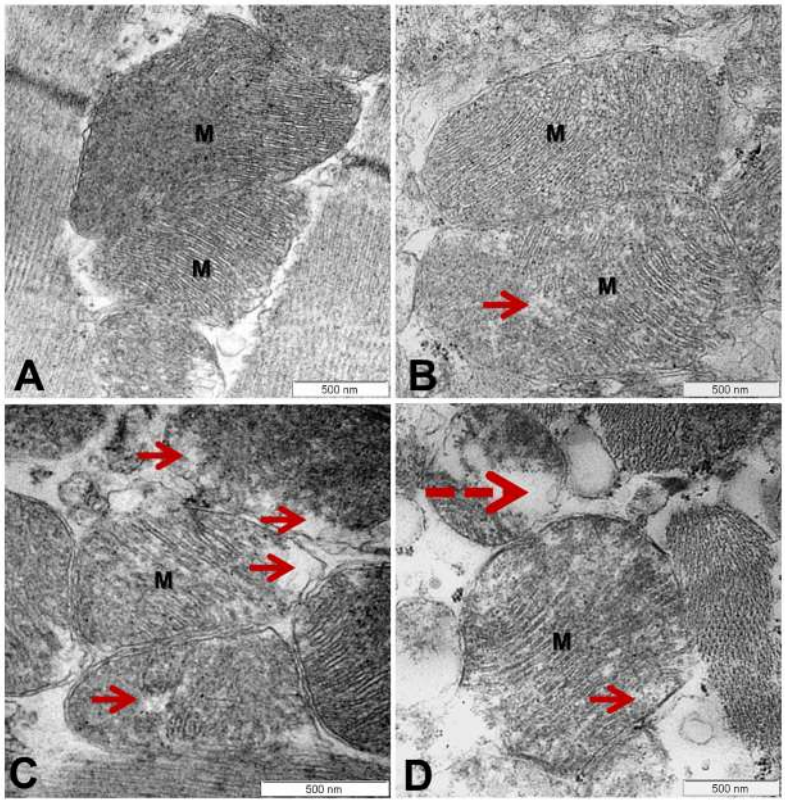

Figure 8: Detailed ultrastructure of cardiomyocyte transverse sections- Figure A (control), Figure B (control treated), Figure C (experimental), and Figure D (experimental treated). M: Mitochondria. Red arrow: Cristae fragmentation. Red dashed arrow: Large amount of cristae fragmentation (Scale bar: 500nm).

Aortic tissue

Following cardiac myofibril observations and comparisons the aortas of the control and experimental groups were conducted. Figures 9 A-D provides a general elastic and collagen fibres overview shown in the control and experimental groups. The control groups showed solid elastic fibres with minor fragmentation points following neighbouring collagen depositions as expected in the aorta. Larger elastic fibre fragmentations and alterations to the standard structure did occur however these were infrequent and minor. While the experimental groups displayed abundant elastin fragmentation and collagen deposition. Elastic fibre fragmentation signified elastic fibre destruction. Where elastin is lost collagen is dispensed. Nevertheless, the remaining elastin band fragments retained their density. The treated experimental group displayed a standard solid elastin band with reduced density. Although, the group displayed a lessened degree of elastin fragmentation and collagen deposition, less collagen fibres were observed around the elastic fibres (figure 9 D).

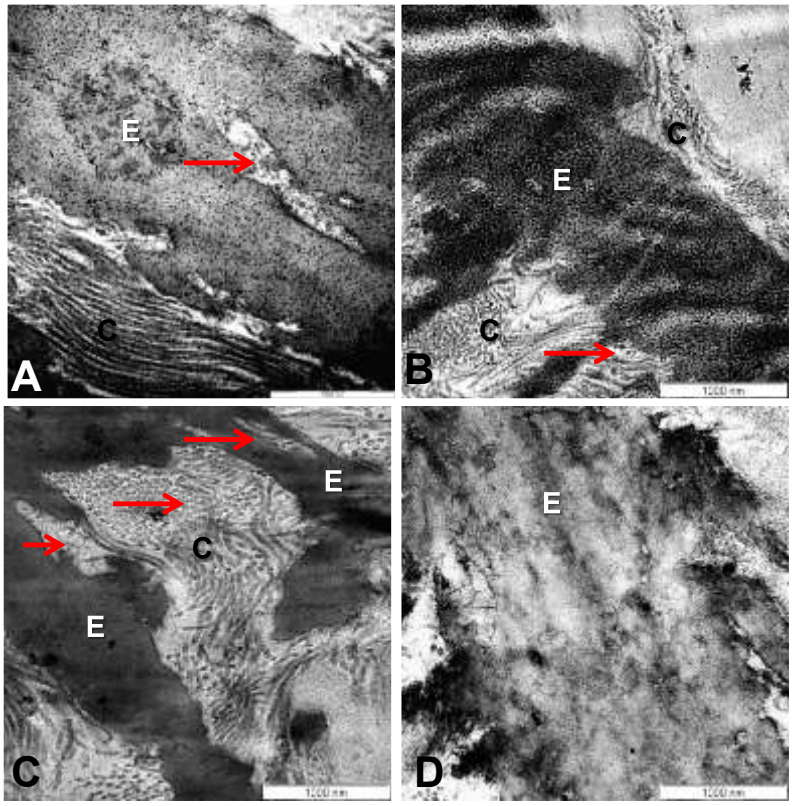

Figure 9: Detailed ultrastructure of aortic transverse sections- Figure A (control), Figure B (control treated), Figure C (experimental), Figure D (experimental treated). C: Collagen fibres, E: Elastic (Scale bars: 1000nm).

Total cholesterol test

The total cholesterol level of each group was analysed using GraphPad Prism 9.0.0. A One-way ANOVA was conducted which compared the mean total cholesterol levels of each testing population. The test found that the total cholesterol levels of the control, treated control, experimental and treated experimental group showed no significant differences. The data is displayed in table 3 and figure 10.

Table 3: Total cholesterol levels- Test groups statistics

Total cholesterol (mg/dl)				
Group	**Mean ± SD**	**Median**	**P-value**	**Significant (yes/no)**
PBS	0,293 ± 0,049	0,289	0,5571	No
PBS + H	0,335 ± 0,090	0,316		
LPS	0,277 ± 0,040	0,270		
LPS + H	0,318 ± 0,067	0,332		

Abbreviations: H: Manuka honey, LPS: Lipopolysaccharide, PBS: Phosphate-buffered saline, SD: Standard deviation

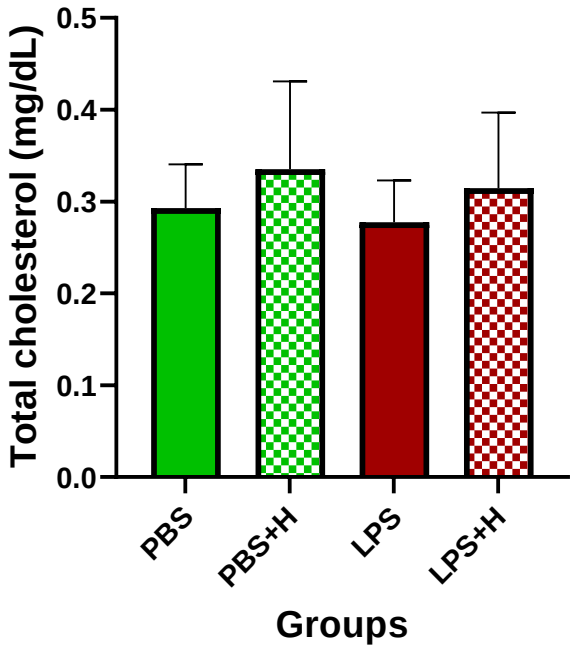

Figure 10: Mean total cholesterol of the control and experimental rat groups- Displays the mean and 95% confidence interval total of the total cholesterol of each test group measured in mg/dL.

Table 4 documents the control, treated control, experimental and treated experimental rat group individual comparisons between each group. The comparison definitively displays that the total cholesterol of the control group shows no statistical significance with the treated control, experimental and treated experimental group. In addition, the other test groups did not display statistical differences to one another.

Table 4: Total cholesterol concentration- Group temperature comparisons

Total cholesterol (mg/dL)			
Groups	Mean difference	P-value	Significant (yes/no)
PBS vs PBS+H	-0,04229	0,8500	No
PBS vs LPS	0,01563	0,9376	No
PBS vs LPS+H	-0,02172	0,9376	No
PBS+H vs. LPS	0,05791	0,7182	No
PBS+H vs LPS+H	0,02056	0,9376	No
LPS vs. LPS+H	-0,03735	0,8643	No

Abbreviations: H: Manuka honey, LPS: Lipopolysaccharide, PBS: Phosphate-buffered saline, SD: Standard deviation

Discussion and Conclusion

In this study, cardiac and aortic tissue evaluations found that the cardiac muscle of LPS exposed animals presented with cardiac myofibril damage and erythrocyte extravasation associated with vascular leakage as a consequence of endothelial damage in some areas (30). While other areas presented with normal cardiac morphology. However, when investigating glycogen accumulation, the experimental groups displayed a lack of glycogen accumulation when compared to the control groups. Therefore, all of the test groups displayed no signs of hypoxia. With the TEM investigation, the LPS treated groups presented with moderate myofibril damage while the addition of the Manuka honey lessened the resulting myofibril damage. Endotoxin exposure also produced mitochondrial cristae damage. Meanwhile, Manuka honey administration failed to counteract the mechanisms involved in the destruction of mitochondria cristae. The study identified that the endotoxin may result in CV toxicity that may cause accelerated CV aging, increased CV disease and thrombotic events. In addition, the observed mitochondrial fragmentation may result in a reduction in mitochondrial respiration leading to an upsurge in mitochondrial oxidative stress and a reduction in membrane potential (31).

When examining the aortic tissue varying tissue disruption in the form of nuclei clustering and flattening in some area was a consequence of endotoxin exposure. In contrast, Manuka honey only presented with aortic tissue damage that presented as perforations that could be observed that the therapeutic remedy neutralised some of the harmful effects of LPS. Regarding the elastic tissue, LPS induced substantial elastic band disruption that was displayed as disordered band arrangements and an excessive number of elastic laminae crosslinks. Elastin depletion may conclude in vasculature stiffening resulting in hypertension and impaired blood flow to vital areas such as the brain, heart, liver and lungs. Manuka honey exposure concluded in a reduction in the elastic band disruption caused by the endotoxin. Upon elastin and collagen inspection using TEM, endotoxin administration concludes in elastin fragmentation and collagen deposition. In contrast, Manuka honey prevents the fragmentation of elastin to a significant degree however, as a consequence the treatment results in collagen depletion. Collagen depletion results in a reduction in the structural integrity of the aorta thus resulting in vascular pathology. Following the total cholesterol analysis, it was concluded that early LPS exposure does not disrupt cholesterol homeostasis.

Nevertheless, Manuka honey is not effective as a mopping agent for systemic inflammation or LPS exposure since the treatment failed to fully counteract the harmful effects of the endotoxin. The study showed that LPS may result in CV complications, however those

complications may result in subclinical symptoms. The study confirmed the relevance of an animal model on the effects of early LPS exposure.

References

1. Irwin MH, Moos WH, Faller DV, Steliou K, Pinkert CA. Epigenetic treatment of neurodegenerative disorders: Alzheimer and Parkinson diseases. Drug development research. 2016;77(3):109-23.
2. Daiber A, Steven S, Weber A, Shuvaev VV, Muzykantov VR, Laher I, et al. Targeting vascular (endothelial) dysfunction. British journal of pharmacology. 2017;174(12):1591-619.
3. Jeon YJ, Jung SJ, Kim HC. Does serum vitamin D level affect the association between cardiovascular health and cognition? Results of the Cardiovascular and Metabolic Diseases Etiology Research Center (CMERC) study. European Journal of Neurology. 2021;28(1):48-55.
4. Katsumoto A, Takeuchi H, Takahashi K, Tanaka F. Microglia in Alzheimer's disease: risk factors and inflammation. Frontiers in neurology. 2018;9:978.
5. Blossom C. M. Stephan SLH, Hannah A. D. Keage, Abrar Babateen, Louise Robinson & Mario Siervo Cardiovascular Disease, the Nitric Oxide Pathway and Risk of Cognitive Impairment and Dementia. Current Cardiology Reports volume 2017;19(87).
6. Troncone L, Luciani M, Coggins M, Wilker EH, Ho C-Y, Codispoti KE, et al. Aβ amyloid pathology affects the hearts of patients with Alzheimer's disease: mind the heart. Journal of the American College of Cardiology. 2016;68(22):2395-407.
7. Li M, Li C, Yu H, Cai X, Shen X, Sun X, et al. Lentivirus-mediated interleukin-1β (IL-1β) knock-down in the hippocampus alleviates lipopolysaccharide (LPS)-induced memory deficits and anxiety-and depression-like behaviors in mice. Journal of neuroinflammation. 2017;14(1):1-12.
8. Katherine R. Hixon SJB, Gabriela Ronning-Arnesen, Blythe E. Janowiak and Scott A. Sell Investigating Manuka Honey Antibacterial Properties When Incorporated into Cryogel, Hydrogel, and Electrospun Tissue Engineering Scaffolds. Cryogelation and Cryogels. 2019;5(2):1-16.
9. Raetz CR, Reynolds CM, Trent MS, Bishop RE. Lipid A modification systems in gram-negative bacteria. Annu Rev Biochem. 2007;76:295-329.
10. Steimle A, Autenrieth IB, Frick J-S. Structure and function: Lipid A modifications in commensals and pathogens. International Journal of Medical Microbiology. 2016;306(5):290-301.
11. Silipo A, Leone MR, Lanzetta R, Parrilli M, Lackner G, Busch B, et al. Structural characterization of two lipopolysaccharide O-antigens produced by the endofungal bacterium Burkholderia sp. HKI-402 (B4). Carbohydrate research. 2012;347(1):95-8.
12. Bai Z, Stamova B, Xu H, Ander BP, Wang J, Jickling GC, et al. Distinctive RNA expression profiles in blood associated with Alzheimer's disease after accounting for white matter hyperintensities. Alzheimer disease and associated disorders. 2014;28(3):226.
13. Xue-Li Lu C-HZ, Han Zhang and Xin-Liang Yao. iRhom2 is involved in lipopolysaccharide-induced cardiac injury in vivo and in vitro through regulating inflammation response. Biomedicine & Pharmacotherapy. 2017;86:645-53.
14. Zhan X, Stamova B, Sharp FR. Lipopolysaccharide Associates with Amyloid Plaques, Neurons and Oligodendrocytes in Alzheimer's Disease Brain: A Review. Frontiers in Aging Neuroscience. 2018;10:42.
15. Subramanian K, Gianni D, Balla C, Assenza GE, Joshi M, Semigran MJ, et al. Cofilin-2 phosphorylation and sequestration in myocardial aggregates: novel pathogenetic mechanisms for idiopathic dilated cardiomyopathy. Journal of the American College of Cardiology. 2015;65(12):1199-214.
16. Huang S, Xu M, Liu L, Yang J, Wang H, Wan C, et al. Autophagy is involved in the protective effect of p21 on LPS-induced cardiac dysfunction. Cell death & disease. 2020;11(7):1-15.
17. Roher AE, Debbins JP, Malek-Ahmadi M, Chen K, Pipe JG, Maze S, et al. Cerebral blood flow in Alzheimer's disease. Vascular health and risk management. 2012;8:599.
18. Nash DT, Fillit H. Cardiovascular disease risk factors and cognitive impairment. The American journal of cardiology. 2006;97(8):1262-5.
19. Jensen HA, Mehta JL. Endothelial cell dysfunction as a novel therapeutic target in atherosclerosis. Expert review of cardiovascular therapy. 2016;14(9):1021-33.

20. Jaw JE, Tsuruta M, Oh Y, Schipilow J, Hirano Y, Ngan DA, et al. Lung exposure to lipopolysaccharide causes atherosclerotic plaque destabilisation. European Respiratory Journal. 2016;48(1):205-15.
21. Tini G, Scagliola R, Monacelli F, La Malfa G, Porto I, Brunelli C, et al. Alzheimer's disease and cardiovascular disease: a particular association. Cardiology Research and Practice. 2020;2020.
22. Bester J, Soma P, Kell DB, Pretorius E. Viscoelastic and ultrastructural characteristics of whole blood and plasma in Alzheimer-type dementia, and the possible role of bacterial lipopolysaccharides (LPS). Oncotarget. 2015;6(34):35284.
23. Ryan KJ. Enterobacteriaceae. Sherris Medical Microbiology, 7e. New York, NY: McGraw-Hill Education; 2017.
24. Bancroft CLaJD. Carbohydrates. Bancroft's Theory and Practice of Histological Techniques. 8: Elsevier; 2019. p. 176-97.
25. G.R H. Techniques in nephropathology. In: S.S. IS, editor. Histochemistry in pathologic diagnosis: New York: Marcel Dekker; 1987.
26. Szymańska E, Szymańska S, Truszkowska G, Ciara E, Pronicki M, Shin YS, et al. Variable clinical presentation of glycogen storage disease type IV: from severe hepatosplenomegaly to cardiac insufficiency. Some discrepancies in genetic and biochemical abnormalities. Archives of medical science: AMS. 2018;14(1):237.
27. Percival K, Radi Z. A modified Verhoeff-van Gieson elastin histochemical stain to enable pulmonary arterial hypertension model characterization. European journal of histochemistry: EJH. 2016;60(1).
28. Viktoryia Kazlouskaya SM, Jennifer Lambe, Munir Hassen Idriss, Dirk Elston, Christian Andres. The utility of elastic Verhoeff-Van Gieson staining in dermatopathology. Journal of Cutaneous Pathology. 2012;40(2):211-25.
29. Lillie RD. histopathologic technic and practical histochemistry McGraw-Hill, editor. New York1965. 1 p.
30. Sharma D, Sharma P, Sharma K, Mathur J, Singh P. Histochemical study of the metabolism and toxicity of mercury. Current Science. 1988;57(9):483-5.
31. Bereketeab Haileselassie RM, Amit U. Joshi, Brooke A. Napier, Liliana M. Massis, Nicolai Patrick Ostberg, Bruno B. Queliconi, Denise Monack, Daniel Bernstein and Daria Mochly-Rosen. Drp1/Fis1 interaction mediates mitochondrial dysfunction in septic cardiomyopathy. Journal of Molecular and Cellular Cardiology. 2019;130:160-9.